AIP | Review of Scientific Instruments

High-resolution tangential absolute extreme ultraviolet arrays for radiated power density measurements on NSTX-Ua)

L. Delgado-Aparicio, R. E. Bell, I. Faust, K. Tritz, A. Diallo, S. P. Gerhardt, T. A. Kozub, B. P. LeBlanc, and B. C. Stratton

Citation: Review of Scientific Instruments **85**, 11D859 (2014); doi: 10.1063/1.4894835
View online: http://dx.doi.org/10.1063/1.4894835
View Table of Contents: http://scitation.aip.org/content/aip/journal/rsi/85/11?ver=pdfcov
Published by the AIP Publishing

Articles you may be interested in

Two-dimensional AXUV-based radiated power density diagnostics on NSTX-Ua)
Rev. Sci. Instrum. **85**, 11D856 (2014); 10.1063/1.4890254

Using X-mode L, R and O-mode reflectometry cutoffs to measure scrape-off-layer density profiles for upgraded ORNL reflectometer on NSTX-Ua)
Rev. Sci. Instrum. **85**, 11D815 (2014); 10.1063/1.4889739

Absolute sensitivity calibration of vacuum and extreme ultraviolet spectrometer systems and Zeff measurement based on bremsstrahlung continuum in HL-2A tokamaka)
Rev. Sci. Instrum. **83**, 10D507 (2012); 10.1063/1.4729671

Development of KSTAR ECE imaging system for measurement of temperature fluctuations and edge density fluctuationsa)
Rev. Sci. Instrum. **81**, 10D930 (2010); 10.1063/1.3483209

10 kHz repetitive high-resolution TV Thomson scattering on TEXTOR: Design and performance (invited)
Rev. Sci. Instrum. **77**, 10E512 (2006); 10.1063/1.2219434

This article is copyrighted as indicated in the article. Reuse of AIP content is subject to the terms at: http://scitationnew.aip.org/termsconditions. Downloaded to IP: 198.125.233.17 On: Mon, 05 Jan 2015 21:13:54

High-resolution tangential absolute extreme ultraviolet arrays for radiated power density measurements on NSTX-U[a)]

L. Delgado-Aparicio,[1] R. E. Bell,[1] I. Faust,[2] K. Tritz,[3] A. Diallo,[1] S. P. Gerhardt,[1] T. A. Kozub,[1] B. P. LeBlanc,[1] and B. C. Stratton[1]
[1]*Princeton Plasma Physics Laboratory, Princeton, New Jersey 08540, USA*
[2]*MIT Plasma Science and Fusion Center, Cambridge, Massachusetts 02139, USA*
[3]*The Johns Hopkins University, Baltimore, Maryland 21209, USA*

(Presented 3 June 2014; received 2 June 2014; accepted 25 August 2014; published online 10 September 2014)

The radiated-power-density diagnostic on the equatorial midplane for the NSTX-U tokamak will be upgraded to measure the radial structure of the photon emissivity profile with an improved radial resolution. This diagnostic will enhance the characterization and studies of power balance, impurity transport, and MHD. The layout and response expected of the new system is shown for different plasma conditions and impurity concentrations. The effect of toroidal rotation driving poloidal asymmetries in the core radiation from high-Z impurities is also addressed. © *2014 AIP Publishing LLC*. [http://dx.doi.org/10.1063/1.4894835]

I. INTRODUCTION AND MOTIVATION

Precise measurements of the local radiated power density and total radiated power are a matter of the uttermost importance for understanding the onset of impurity-induced instabilities and the study of particle and heat transport. Accounting of power balance is also needed for understanding the physics of various divertor configurations for present and future high-power fusion devices. Poloidal asymmetries in the impurity density can result from high Mach numbers and can impact the assessment of their flux-surface-average and hence vary the estimates of $P_{rad}(r, t)$ and $\langle Z_{eff}\rangle$; the latter is used in the calculation of the neoclassical conductivity and the interpretation of non-inductive and inductive current fractions. To this end, the bolometric diagnostic in NSTX-U will be upgraded, enhancing the midplane coverage and radial resolution with two tangential views, and adding a new set of poloidally-viewing arrays to measure the 2D radiation distribution.[1] These systems are designed to contribute to the near- and long-term highest priority research goals for NSTX-U which will integrate non-inductive operation at reduced collisionality, with high-pressure, long energy-confinement-times, and a divertor solution with metal walls.

II. INSTRUMENTATION

Bolometers are detectors that can measure radiation over a broad spectrum from the soft x-rays ($\lambda_{SXR} \gtrsim 1$ Å) to the infrared ($\lambda_{IR} \sim 1000$Å) with a nearly uniform sensitivity at all wavelengths. In this paper, we discuss a the design of a radiometer diagnostic system based on silicon photodiode detectors (AXUV absolute extreme ultraviolet) from Opto Diode Corp. (formerly International Radiation Detectors Inc.[2]). NSTX's previous 16-channel midplane array[3] will be replaced by two unbiased AXUV20, 40-elements diode array. This compact diagnostic will be installed at the equatorial midplane of a tangential port and will measure the radial structure of the photon emissivity profile in order to perform edge and core power balance, as well as impurity transport and MHD studies. These photodiodes feature a nearly "flat" spectral responsivity of $\mathcal{R}_0 \sim 0.275$ A/W for photon energies of 0.2 and 5 keV; the quantum efficiency loss (mainly for 7–100 eV photons) is due to the front radiation-hard silicon dioxide window since oxide absorption and reflections are not negligible. They have an active surface area of 0.75×4.1 mm and an intrinsic 10%–90% rise time of 0.2 μs. The new systems will provide several advantages over the prior AXUV implementation including increased dynamic range and a remote-controlled gain which can be adjusted in real time. Standard transimpedance amplifiers using the built-in variable gains of the MAZeT IC can be manually set using toggle switches or controlled via digital programming using the data acquisition system.[4] Eight different bandwidths and gains can be set from 2.5×10^5 V/A with a bandwidth of 300 kHz to 2×10^8 V/A with a corresponding bandwidth of 6 kHz. Voltages will be digitized using a 16 bit D-tAcq ACQ196CPCI-96-500 data acquisition module which supports 96 simultaneous channels of 16-bit analog-to-digital conversion with a 500 kHz sampling rate and a ± 10 V full scale input range.

III. SYNTHETIC DIAGNOSTIC

The new arrays will measure line and continuum emission from the plasma with photon energies of few eV up to 10 keV, therefore the signal to noise ratio will depend strongly on the local electron and impurity density as well as the plasma temperature. A synthetic diagnostic capability has been built to estimate the response of both, the 1D tangential AXUV diode array reported here, and the 2D poloidally viewing system described in a different paper in these conference

[a)]Contributed paper, published as part of the Proceedings of the 20th Topical Conference on High-Temperature Plasma Diagnostics, Atlanta, Georgia, USA, June 2014.

 © 2014 AIP Publishing LLC

This article is copyrighted as indicated in the article. Reuse of AIP content is subject to the terms at: http://scitationnew.aip.org/termsconditions. Downloaded to IP: 198.125.233.17 On: Mon, 05 Jan 2015 21:13:54

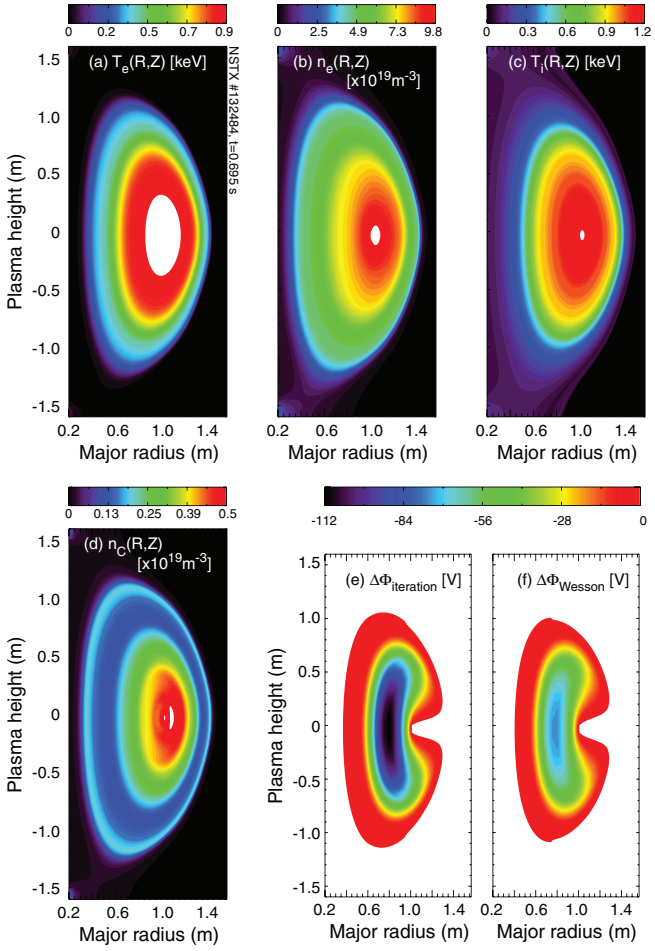

FIG. 1. NSTX 2D profiles of (a) T_e, (b) n_e, (c) T_C, and (d) n_C. A comparison between the numerical solution for the electrostatic potential ($\Delta\Phi$) with that of the analytical formula by Wesson are shown in (e) and (f), respectively.

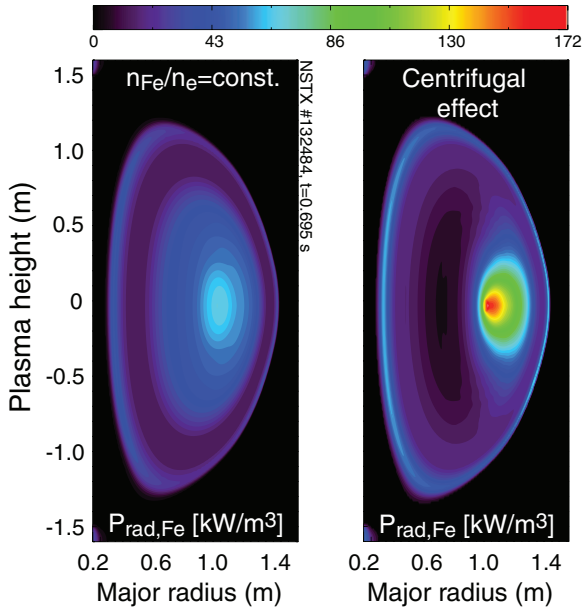

FIG. 2. 2D synthetic iron radiated power densities for a total radiated power of 1 MW. The two cases shown consider a constant iron concentration across the plasma cross section and the effect of centrifugal forces.

proceedings.[1] The local radiated power density profiles have been modeled using hydrogenic Bremsstrahlung and cooling rates for the intrinsic impurities of choice (e.g., C and Fe) according to

$$P_{rad}(R, Z, t) = n_e n_D L_D + \sum n_e n_Z L_Z(T_e), \qquad (1)$$

where, n_e, n_D, and n_Z are the electron, deuterium, and impurity densities, respectively; $L_D = 5.35 \times 10^{-37} T_e^{1/2}$[keV] W m^3 is the hydrogenic Bremsstrahlung, while the L_Z considered – in a first approximation – are the temperature-dependent steady-state radiative cooling rates tabulated by Post and Jensen.[5]

The 2D maps of electron and carbon temperature shown in Fig. 1 were obtain using an EFIT reconstruction routine with the assumption that the plasma temperatures are a flux-surface functions. Mid-plane measurements of the aforementioned quantities were done using the Multi-Point Thomson Scattering[6] and the Charge Exchange Recombination Spectroscopy[7] diagnostic systems. The 2D electron, deuterium, and carbon densities were obtain self-consistently assuming the presence of a poloidal variation of particle density due to centrifugal forces.[8] The solutions for the 2D density maps assuming a distribution of the form $n_j = n_{j,0} \exp(\frac{\frac{1}{2} m_j \omega^2 (R^2 - R_0^2) - e Z_j \Delta\Phi}{k_B T_j})$ for an arbitrary carbon density, in the limit of a zero electron mass and $T_D = T_C$ are shown in Fig. 1. The solution for the electrostatic potential for the measured carbon density and a modest central toroidal rotation of 190 km/s ($f_{\phi,0} \sim 28$ kHz) is shown in Fig. 1(e); the values of $\Delta\Phi$ using Wesson's formalism (assuming that the main intrinsic impurity is in the trace limit) underestimate the electrostatic potential by 60%–70% [see Fig. 1(f)]. The presence of iron as the extrinsic impurity of choice is modeled on the trace limit with very small changes to quasineutrality and Z_{eff}. The results for the iron radiated power distributions assuming two distinct cases with a constant iron fraction and the effect of centrifugal forces are depicted in Fig. 2. A detailed treatment of this work will be described in a different publication elsewhere.

IV. INSTRUMENT COVERAGE AND RESPONSE

Only the details from the core tangential midplane system shown in Fig. 3 will be outlined in this paper. As shown below the two-diode tangential array view will share the available space in a tangential port with the NSTX-U multi-energy SXR array.[4] These AXUV-based systems will use a mechanical shutter to protect the pinhole slits and the diodes from deposits occurred during Li-evaporation, boronization as well as He/Ne GDC.

The power deposited in each of the tangential-viewing AXUV diodes will be measured by an electrical signal that can be calculated using

$$\mathcal{S}_i[\mathrm{V}] = G_1\left[\frac{V}{A}\right] G_2\left[\frac{V}{V}\right] \mathcal{R}_0\left[\frac{A}{W}\right] \frac{\eta[m^2 str]}{4\pi} B_i\left[\frac{W}{m^2}\right], \qquad (2)$$

This article is copyrighted as indicated in the article. Reuse of AIP content is subject to the terms at: http://scitationnew.aip.org/termsconditions. Downloaded to IP: 198.125.233.17 On: Mon, 05 Jan 2015 21:13:54

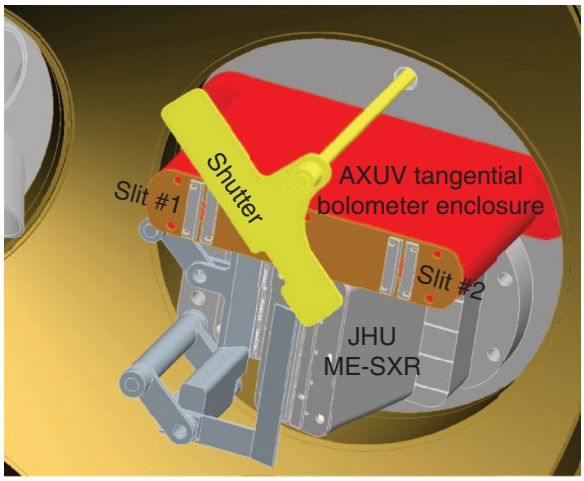

FIG. 3. Top view of re-entrant high-resolution tangential AXUV diode system designed for NSTX-U.

where G_1 is the first stage transimpedance amplifier gain, G_2 is the 2nd stage voltage amplifier circuits with low output impedance capable of driving the cabling used to deliver the AXUV signals to the data acquisition system, $\mathcal{R}_0$ is the ideal diode responsivity and η is the *etendue* of the system. The integrated brightness is given by $B_i = \int E_j \cdot dl_i$, where E[W/m^3] is the local radiated power density or emissivity and dl[m] is a line-element along the detector sightline. Because the emission from toroidal, axisymmetric plasmas has circular symmetry, the tangential, line-integrated profiles can be inverted using the standard one-dimensional 1D Abel equation. The matrix-based inversion technique used hereafter has been described by Bell,[9] and has already been applied to both tangential imaging of charge exchange recombination spectroscopy,[7] hard[9] and soft[10,11] x-rays and bolometric measurements.[3,12] In such formalism the brightness and inverted emissivity can be easily expressed as

$$B_i = \sum_j \mathcal{L}_{ij} E_j \Rightarrow E_j = \sum_i \mathcal{L}_{ji}^{-1} B_i. \quad (3)$$

As shown in Fig. 4, both the emissivity and the integrated brightness profiles are sensitive to the presence of impurity in/out asymmetries due to centrifugal effects. For various NSTX H-mode scenarios the peak emissivity and brightness can be as high as 0.3 MW/m^3 and 0.5 MW/m^2 which will correspond to measured photo-currents and voltages up to 15 μA and Volts ($G_1 G_2 = 10^6$ V/A), respectively. This versatile design will allow the study of CHI, Ohmic, RF, and NBI-heated plasmas.

V. CORRECTING FOR NONLINEAR RESPONSIVITY

As discussed above the AXUV efficiency is highly nonlinear in the range of 1–100 eV in comparison to its nearly

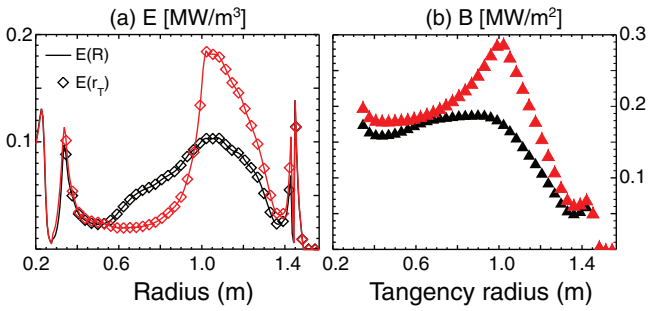

FIG. 4. (a) and (b) Midplane emissivity and integrated brightness calculations for the cases shown in Fig. 2.

constant responsivity for energies above 200 eV. Several diagnostics show high edge carbon (CIII, CIV, and CVI radiation) emission that peaks within 2–3 cm of the separatrix. The response to photons in the 8–12 eV range (characteristic of CIII-12.7 eV and CIV-8.0 eV) is, on average, 2.6 times less sensitive than photons with energies >50 eV. A first approach to compensate for this lack of detector sensitivity will be to multiply the inverted emissivities of the outer plasma (e.g., ~3 cm inside the separatrix) by this factor of 2.6. A second method consists on assuming that the average photon energy emitted scales as the local electron temperature or as a function of the latter. Either way, $\mathcal{R}^* = \mathcal{R}/\mathcal{R}_0$ is the ratio of the "local" to the ideal responsivity and the brightness and inverted emissivity calculations can be expressed as

$$B_i = \sum_j \mathcal{L}_{ij} E_j \mathcal{R}_j^*(T_{e,j}) \Rightarrow E_j = \frac{1}{\mathcal{R}_j^*} \sum_i \mathcal{L}_{ji}^{-1} B_i. \quad (4)$$

This novel approach will be tested first using the NSTX database and will implemented later for NSTX-U radiated power density measurements. This work was performed under US DOE Contract Nos. DE-FC02-99ER54512 at MIT and DE-AC02-09CH11466 at PPPL.

[1]I. Faust, L. Delgado-Aparicio *et al.*, Rev. Sci. Instrum. **85**, 11D856 (2014).
[2]See http://optodiode.com/ for information on diode array.
[3]S. F. Paul *et al.*, J. Nucl. Mater. **337–339**, 251 (2005).
[4]K. Tritz *et al.*, Rev. Sci. Instrum. **83**, 10E109 (2012).
[5]D. E. Post and R. V. Jensen, At. Data Nucl. Data Tables **20**, 397 (1977).
[6]B. P. LeBlanc *et al.*, Rev. Sci. Instrum. **74**, 1659 (2003).
[7]R. E. Bell and R. Feder, Rev. Sci. Instrum. **81**, 10D724 (2010).
[8]J. A. Wesson, Nucl. Fusion **37**, 577 (1997).
[9]R. E. Bell, Rev. Sci. Instrum. **66**, 558 (1995).
[10]L. Delgado-Aparicio *et al.*, J. Appl. Phys. **102**, 073304 (2007).
[11]L. Delgado-Aparicio *et al.*, Plasma Phys. Control. Fusion **49**, 1245 (2007).
[12]M. L. Reinke *et al.*, Rev. Sci. Instrum. **79**, 10F306 (2008).

This article is copyrighted as indicated in the article. Reuse of AIP content is subject to the terms at: http://scitationnew.aip.org/termsconditions. Downloaded to IP: 198.125.233.17 On: Mon, 05 Jan 2015 21:13:54